Atmos. Chem. Phys. Discuss., 10, 69–108, 2010
www.atmos-chem-phys-discuss.net/10/69/2010/


Atmospheric Chemistry and Physics Discussions

This discussion paper is/has been under review for the journal Atmospheric Chemistry and Physics (ACP). Please refer to the corresponding final paper in ACP if available.

# Characteristics of size distributions at urban and rural locations in New York

**M.-S. Bae[1], J. J. Schwab[1], O. Hogrefe[1], B. P. Frank[2], G. G. Lala[1], and K. L. Demerjian[1]**

[1]Atmospheric Sciences Research Center, University at Albany, State University of New York, Albany, New York, USA
[2]Division of Air Resources, New York State Department of Environmental Conservation, Albany, NY, USA

Received: 4 September 2009 – Accepted: 8 December 2009 – Published: 5 January 2010

Correspondence to: M.-S. Bae (minsbae@hotmail.com)

Published by Copernicus Publications on behalf of the European Geosciences Union.

## Abstract

Paired nano- and long-tube Scanning Mobility Particle Sizer (SMPS) systems were operated for four different intensive field campaigns in New York State. Two of these campaigns were at Queens College in New York City, during the summer of 2001 and the winter of 2004. The other field campaigns were at rural sites in New York State.

The data with the computed diffusion loss corrections for the sampling lines and the SMPS instruments were examined and the combined SMPS data sets for each campaign were obtained. The diffusion corrections significantly affect total number concentrations, and in New York City, affect the mode structure of the size distributions. The relationship between merged and integrated SMPS total number concentrations with the diffusion loss corrections and the CPC number concentrations yield statistically significant increases (closer to 1) in the slope and correlation coefficient compared to the uncorrected values. The measurements are compared to $PM_{2.5}$ mass concentrations and ion balance indications of aerosol acidity. Periods of low observed $PM_{2.5}$ mass, high number concentration, and low median diameter due to small fresh particles are associated with primary emissions for the urban sites; and with particle nucleation and growth for the rural sites. The observations of high $PM_{2.5}$ mass, lower number concentrations, and higher median diameter are mainly due to an enhancement of coagulation and/or condensation processes in relatively aged air. There are statistically different values for the condensation sink (CS) between urban and rural areas. While there is good association ($r^2$>0.5) between the condensation sink (CS) in the range of 8.35–283.9 nm and $PM_{2.5}$ mass in the urban areas, there is no discernable association in the rural areas. The average (±standard deviation) of CS lies in the range $6.5(\pm3.3)\times10^{-3}$–$2.4(\pm0.9)\times10^{-2}$.

## 1 Introduction

Atmospheric aerosols are ubiquitous in the Earth's atmosphere and affect our quality of life through many different processes (Hopke, 2009). As additional information comes to light concerning the role of nano particles in aerosol formation and growth, in manufacturing and nanotechnology, in human health effects, and in climate; the measurements of size distributions inclusive of particles in ultrafine (<100 nm) as well as accumulation (>100 nm) size range, while always important and of interest, have gained increasing attention (Buonanno et al., 2009; Chow et al., 2005; Kulmala et al., 2004a; McMurry, 2000; McMurry et al., 1996; Qian et al., 2007; Watson et al., 2006). Understanding potential hazards of nano particles will require the ability to determine not only their chemical nature but also their size, shape, and number. A standard dose metric for nano particles, whether surface area or particle number or some other quantity, would facilitate cross-comparisons between toxicity studies and exposure measurements (Su et al., 2008; Dall'Osto et al., 2008).

Nanotechnologies encompass broad interdisciplinary areas of research, development, and industrial activity that have been growing rapidly for the past decade. Disciplines include areas of physics, chemistry, biology, engineering, and electronics. Measuring as particles these entities that consist of as few as 200–300 molecules is also a significant challenge, both in terms of detection sensitivity and in terms of sample handling (Hinds, 1982; Brockman, 2001; Wang et al., 2002). Diffusion losses are inevitable in any measurement system involving sample lines, and will generally have a greater impact on the measured concentrations than on the mean particle size, but can also cause the measured size distribution to shift towards larger diameters. Such diffusion losses in the SMPS have been observed in experiments conducted with polydisperse NaCl aerosol in laboratory conditions (Frank et al., 2008). Losses were shown to occur in various parts of the Electrostatic Classifier. Other investigators have also found significant diffusion losses occurring within the Differential Mobility Analyzer (DMA) portion of the SMPS (Reineking and Porstendörfer, 1986; Rodrigue et al., 2007;

Jeong and Evans, 2009).

In the atmosphere, the mechanisms of nano particle formation/growth remain a research topic of great interest (Zhang et al., 2004). Observations of enhanced particle number concentrations (or particle bursts) may be due to either new particle growth and formation; or to the transport of the particles to the observation site. The formation of ultrafine particles detected at a few nm, and subsequent growth to >50 nm in days, has been observed frequently (Dal Maso et al., 2005; Jeong et al., 2004; Kulmala et al., 2004a; Stanier et al., 2004). Competing with the formation and growth of new detectable particles is the condensation of clusters and gases onto pre-existing particles. This process is parameterized by a derived quantity called the condensation sink, which is a useful concept in the evaluation of atmospheric aerosol dynamics (Lehtinen et al., 2003).

This work presents measurements of particle number concentrations and size distributions obtained using two SMPSs: one with a Nano Differential Mobility Analyzer (Nano SMPS) and another with a long-tube Differential Mobility Analyzer (LDMA SMPS). Measurements were conducted at the sites of Whiteface Mountain (WFM, summer 2002) and Pinnacle State Park (PSP, summer 2004) in rural areas of New York State and at the urban site of Queens College (QC) in New York City in summer 2001 and winter 2004. The size distribution measurements were complemented by the total number concentration measurements obtained using co-located Condensation Particle Counters (CPC). This study examines the effect of the diffusion loss corrections for the sampling lines (from ambient inlet to each instrument) and the SMPS by current TSI diffusion loss correction method on these measurements, then provides a comprehensive picture of the evolution of the urban/rural aerosol and examines the physical processes leading to changes in the number size distribution and in the condensation sink.

## 2 Experimental methods and data analysis

### 2.1 Measurement locations and periods

Measurements of particle number concentrations and size distributions during four intensive field studies were performed using a stand-alone Condensation Particle Counter (CPC) and two Scanning Mobility Particle Sizers (SMPS). One of the SMPS instruments utilized a Nano Differential Mobility Analyzer (Nano SMPS) and with the other utilized a long-tube Differential Mobility Analyzer (LDMA SMPS). Table 1 summarizes operational parameters for the particle sizing and counting instruments. The Nano SMPS and LDMA SMPS were operated at Queens College (QC) in New York City from 3 July to 5 August 2001 and from 10 January to 5 February 2004; at Whiteface Mountain (WFM) from 10 July to 7 August 2002 and at Pinnacle State Park (PSP) from 13 July to 6 August 2004. These campaigns will be referred to as QC01, QC04, WFM02, PSP04, respectively.

Queens College (QC), the urban site, is located in a high population density section of New York City and has two busy highways nearby – the Long Island Expressway (I-495) and the Van Wyck Expressway (I-678). Whiteface Mountain (WFM) lodge site is halfway up the mountain at an elevation of about 600 m above sea level (a.s.l.), is surrounded by forest and mountains and located in the Adirondack Park of Northern New York State. Pinnacle State Park (PSP), the other rural site, is at an elevation of about 500 m a.s.l. and is located in southwestern New York in the low population density rural village of Addison, surrounded by light residential neighborhoods, parklands, and forested areas. Detailed descriptions of site operations and locations can be found elsewhere (Schwab et al., 2004, 2006).

### 2.2 Condensation Particle Counter (CPC)

A stand-alone Condensation Particle Counter (CPC, TSI Model 3022) was used to measure the number concentrations of particles at the four sampling sites. Instrument

specifications indicate a 50% detection efficiency for a particle diameter of 7 nm ($D_{50}$) and a 90% detection efficiency at particle diameter of 15 nm. 5-min averaged concentrations were recorded during the QC01, QC04 and PSP04 campaigns, and 10-s measurements were recorded during the WFM02 campaign (subsequently averaged to 5 min).

### 2.3 Scanning Mobility Particle Sizers (SMPSs)

The Nano SMPS components were an Electrostatic Classifier (TSI Model 3080), Nano DMA (TSI Model 3085) and a CPC (TSI Model 3025). The LDMA SMPS consisted of an Electrostatic Classifier (TSI Model 3080), Long-tube DMA (TSI Model 3081) and a CPC (TSI Model 3010 or CPC 3025). Operational details for these instruments during the four campaigns are summarized in Table 1.

#### 2.3.1 Diffusion loss for the sampling lines

Sample line diffusion loss caused by particle deposition onto sample lines is expected. In order to estimate the diffusion losses in the sampling lines, an equation for circular tube penetration efficiency for aerosols can be derived (Hinds, 1981).

$$P = \frac{n_{\text{out}}}{n_{\text{in}}} = 1 - 5.50\mu^{2/3} + 3.77\mu \tag{1}$$

$$\mu = \frac{DL}{Q} \tag{2}$$

The penetration $P$ as a function of $\mu$ (a dimensionless deposition parameter) can be expressed by Eq. (1). In Eq. (2), $D$ (size dependent) is the particle diffusion coefficient, $L$ is the length of the sampling lines, and $Q$ is the volume flow rate through the sampling lines.

### 2.3.2 Diffusion loss for the SMPS

The diffusion losses are characterized in terms of total penetration, which for the SPMS is the product of the penetration for five composite flow paths through the SMPS: impactor inlet, bi-polar neutralizer and the internal plumbing, the tubing to the DMA and CPC, the DMA itself, and the CPC (including penetration inside the CPC, activation and optical detection efficiencies and CPC inlet losses). Particle losses due to diffusion are more pronounced at lower flow rates and for smaller particles (Frank et al., 2008). A diffusion loss correction, which has recently been incorporated into a software module for the TSI SMPS (Aerosol Instrument Manager, ver 8.0, TSI, 2006) and allows particle size distributions for existing SMPS data to be recalculated to account for diffusion losses in the instrument, is applied for the Nano and LDMA SMPS datasets.

## 2.4 Condensation sink (CS)

The aerosol condensation sink (CS) is a measure of how rapidly molecules (and clusters) will condense onto preexisting aerosols (Dal Maso et al., 2002; Lehtinen et al., 2003; Pirjola et al., 1999).

An expression for the condensation sink (CS), with unit of $s^{-1}$, describes the loss rate of molecules with diameter $dp$, diffusion coefficient $D$, onto a distribution $n(d_p)$ or $Ni$ of existing aerosols. Thus, the CS can be calculated by integrating or summing over the size spectrum from SMPS data;

$$\begin{aligned} \mathrm{CS} &= 2\pi D \int_0^\infty d_p \beta_M(d_p) n(d_p) d d_p \\ &= 2\pi D \sum_i \beta_{Mi} d_{p,i} N_i \end{aligned} \tag{3}$$

In Eq. (3), the diffusion coefficient $D$ is typically taken as that of $H_2SO_4$ in air (Hanson and Eisele, 2000), and the transitional correction factor $\beta_M$ can be expressed as (Fuchs

and Sutugin, 1971);

$$\beta_M = \frac{K_n + 1}{0.377K_n + 1 + \frac{4}{3}\partial^{-1}K_n^2 + \frac{4}{3}\partial^{-1}K_n} \tag{4}$$

In Eq. (4), $\partial$=1 is the sticking coefficient (Paul et al., 2004), and the Knudsen number $K_n$ can be expressed in terms of particle diameter and the mean free path of vapor molecules ($\lambda_v$) as (Pirjola et al., 1999);

$$K_n = \frac{2\lambda_v}{d_p} \tag{5}$$

The mean free path $\lambda_v$ in Eq. (5) can be determined from the following formula from Willeke (1976).

$$\lambda_v = \lambda_r \left(\frac{101}{P}\right)\left(\frac{T}{293}\right)\left(\frac{1 + 110/293}{1 + 110/T}\right) \tag{6}$$

where $P$ is in kPa and $T$ in K. In air at 293 K and atmospheric pressure, the mean free path $\lambda_r$ is 0.0664 µm, the factor of 110 (K) is the Sutherland constant. Using this reference value, $\lambda_v$ can be determined for observed pressures and temperatures at the sampling sites. Using these values, and our measured size distributions, values for the condensation sink were computed for the four campaigns.

## 3 Results and discussion

### 3.1 Diffusion loss correction for the sampling lines

Figure 1 shows the percent of diffusion losses for the sampling lines for the Nano SMPS and LDMA SMPS. When the Nano SMPS is set up with a 5.0 l/min bypass flow the integrated total average of the diffusion losses for the sampling lines was less than 2%

for WFM02, so these diffusion losses in the sampling lines are almost negligible for total aerosol nano particle number concentrations. However, since the diffusion losses are size dependent (the smaller the particle the more susceptible it is to diffusion. These losses cannot be ignored when sizing nano particle aerosols.

### 3.2 Diffusion loss correction for the SMPS-empirical transfer function

All data was originally analyzed after the measurement campaigns using TSI software available at that time, which did not include the diffusion correction option. The effects of the diffusion correction on the data sets are presented below, but unless otherwise noted, all data used has been recalculated with the updated software to compensate for diffusion losses (in addition to the standard multiple charging correction).

Recovery of an aerosol size distribution from particle counts recorded during SMPS measurements can be described in terms of the instrument empirical transfer function, which operationally produces the reported number of particles in a given bin (dN) from the raw number of particle counts measured by the CPC (dC). That is, the empirical transfer function is given by $dN/dC$, or more precisely as $\Delta N/\Delta C$. In Fig. 2 we present the empirical transfer function with and without the diffusion correction for the SMPS, and the diffusion correction factors themselves. These quantities in Fig. 2 are computed for two periods encompassing 10 size distributions for each campaign. (For the QC campaigns, a size distribution is derived from a single 2.5 min SMPS scan, while for the WFM and PSP campaigns two 2.5 min SMPS scans are averaged to derive each size distribution.) The periods were chosen to represent moderate to high number concentrations ($cm^{-3}$) for the campaign, and to explore possible sensitivity of the correction to varying concentrations and particle distributions. Table 2 shows the number concentrations in size range for empirical transfer function for the Nano SMPS.

While $\Delta N/\Delta C$ ratios for different time periods within a single field campaign do not vary significantly, the results shown in Fig. 2a – diffusion correction applied – and b – without the diffusion correction – indicate that the $\Delta N/\Delta C$ ratio depends upon sampling site, and in particular upon the total number concentration and the SMPS flow rates.

Any increase in the DMA sample flow means a larger fraction of the particles in the sample are being detected due to reduction of diffusion losses by virtue of a reduced residence time. Figure 2c shows the contribution of the diffusion correction only to the empirical transfer function ($\Delta N/\Delta C$). For our conditions, the diffusion correction is 12–15% at 100 nm, increases to about a factor of two at 20 nm, then increases rapidly with decreasing diameter, reaching values at the lowest reported mobility diameters of almost eight for SMPS flow of 0.3 lpm and between four and five for SMPS flow of 0.6 lpm.

The rapidly increasing diffusion correction presents a dilemma for those trying to obtain size distributions for particles down to very small sizes. Clearly the correction is necessary to produce reliable data for sizes on the order of 20 nm or smaller. However, applying the correction to the very smallest size bins in our campaigns (below 8 nm in our campaigns) produced sporadic and noisy data. This is because the diffusion correction, and by extension the empirical transfer function ($\Delta N/\Delta C$) becomes so large (as big as 20 000–30 000) that single counts in the smallest size bins become significantly over emphasized resulting in unrealistic particle size distributions. We compromised by only considering sizes above 8 nm, which unfortunately required excluding data for smaller size bins.

### 3.3 Relationship between Nano SMPS and LDMA SMPS

Both the Nano SMPS and LDMA SMPS data presented here have been recalculated to include both diffusion loss correction for the sampling lines and diffusion loss correction for the SMPS. Since we want to combine the two SMPS systems to provide a full size distribution of sub-micron particles after the diffusion corrections, the first task is identifying a legitimate merge size point between the Nano SMPS and LDMA SMPS. Figure 3a shows how the merge size points were chosen. We calculated the coefficient of determination ($r^2$ value) for Nano and LDMA SMPS size bins centered on a range of mobility diameters from less than 30 nm to more than 80 nm. For each campaign, the mean bin diameter corresponding to the largest $r^2$ value between the Nano and LDMA

data sets was chosen as the merge point. A merge point of 62.6 nm was determined for the QC01, WFM02, and QC04 campaigns. A different merge point of 37.9 nm was determined for the PSP04 campaign due to a noticeable discontinuity in mean value at 62.6 nm; namely, the Nano SMPS data yielded concentrations in the size bin about 30% lower than LDMA data. If we were to choose 62.6 nm as the merge point for PSP04 campaign the total integrated number concentration from the combined SMPS measurements would be about 5% lower. The best explanation we have is that the different merge point for the PSP04 campaign could be due to different operation conditions.

As can be seen for Table 3, the size bins are nearly identical in width and location for the Nano and LDMA systems in the overlap region. Figure 3b shows the relationships between hourly averaged LDMA SMPS [62.6 nm] and Nano SMPS [62.6 nm] number concentrations for the QC01, WFM02, and QC04 campaigns, and between hourly averaged LDMA SMPS [37.9 nm] and Nano SMPS [37.9 nm] number concentrations for the PSP04 campaign. The linear correlations between Nano SMPS and LDMA SMPS yield good correlations ($r^2$ of >0.9) for all campaigns except QC01 ($r^2$ of 0.89). We attribute the lower correlation for the QC01 campaign to two factors: 1) the Nano SMPS and LDMA SMPS inlets were approximately 10 m from each other and the inlet designs were different for these measurements; and 2) the LDMA SMPS flow conditions were varied numerous times during the campaign. The correlations between merge point bins Nano SMPS and LDMA SMPS for QC01, WFM02, and PSP04 have slopes of 1.00, 0.96, and 0.97, respectively. The correlation for QC04 is significantly different from the other campaigns with a slope of 0.80. The Nano SMPS at the QC04 campaign yields higher values than the LDMA SMPS for sizes less than 100 nm. We do not clearly understand why the QC04 Nano and LDMA data show poorer agreement than the other three campaigns, but simply note that it was the only campaign that occurred during the winter.

### 3.4 Relationship between SMPS and CPC total concentrations

The hourly averaged SMPS (8.35–283.9 nm) with and without diffusion loss corrections and CPC data with diffusion loss correction were compared for all sampling periods. These pairwise correlations provide insight into the range of each measurement, allow comparisons between the instruments, and demonstrate the effect of recalculating the data to account for diffusion losses. Note that CPC data were corrected for the diffusion loss in the sampling lines as well, but since we have no size information from the CPC itself, we assumed the particles to have the same size distributions as Nano SMPS. Total averages of the diffusion losses for the CPC yield less than 4% losses for all four campaigns.

Figure 4 shows the pairwise correlation scatterplots for CPC and SMPS, and their corresponding average size distributions measured by the Nano SMPS for the a) QC01, b) WFM02, c) QC04, and d) PSP04 campaigns. One hour averages were calculated only for those hours for which 75% or more data were available.

The SMPS number concentrations (diffusion loss corrections both for the sampling lines and the SMPS, 8.35–283.9 nm) and the CPC (diffusion loss correction for the sampling lines) number concentrations agree well for the four campaigns with linear regression slopes of 0.76–1.13 (forced to zero) and $r^2$ of 0.59–0.97. The correlation values for the QC01 campaign are lower than those for the other campaigns due to varying sampling conditions as discussed previously. As seen in the Fig. 4, when the diffusion loss corrections are applied to the data, all four campaigns yield statistically significant increases (closer to 1) in the slope and correlation coefficient ($r^2$). This is a strong indication that applying the diffusion loss corrections produced a better representation of the ambient particle concentrations.

### 3.5 Nano particle size distributions at urban and rural locations in New York

The right panels of Fig. 4 shows the average Nano SMPS size distributions measured by the Nano SMPS for the QC01, WFM02, QC04, and PSP04 campaigns. There are

markedly different size distribution shapes (both before and after diffusion loss corrections) between the urban and rural locations. For the WFM02 campaign, the average number size distribution has a broad peak at about 50 nm; while the PSP04 campaign distribution shows a gradual increase (no clear mode in Nano SMPS). These features at the rural sites are the same both with and without diffusion loss corrections. However, for both the QC01 and QC04 campaigns, the average number size distribution has a clear mode at approximately 13 nm when corrected for diffusion loss. This is a significantly lower mode diameter than appears in the distribution prior to diffusion loss corrections, and indicates a much more dynamic situation at the QC site.

In general, for ambient aerosols at rural sites (WFM02 and PSP04), the diffusion loss corrections affect the absolute values of the particle concentrations but not the mode diameter or basic shape of the size distribution. Thus, in some instances, the diffusion loss corrections may not be necessary when only examining relative trends in the rural locations that experience predominantly well-aged particles. For ambient aerosols at our urban campaigns (QC01 and 04), the diffusion loss corrections affect both the absolute values of the particle concentrations and the basic shape of the size distribution. We believe these results show that diffusion loss corrections are always necessary for SMPS data gathered from an urban location. These findings may be useful when evaluating whether reprocessing extremely large data sets from rural or urban ambient monitoring sites will yield important additional information.

### 3.6 Statistical characteristics of the measurements

Figure 5 and Table 4 show the measurement locations and the statistical characteristics of hourly averaged number concentrations measured by CPC and diffusion loss corrected SMPS at the four sampling sites. The hourly average of CPC and SMPS number concentrations, rounded to three significant figures, are 22 100±10 700 1/cm$^3$ (average±standard deviation) and 24 100±10 700 1/cm$^3$, respectively for the QC01, and 87 600±26 900 1/cm$^3$ and 66 800±22 600 1/cm$^3$, respectively for QC04. Winter particle concentrations at QC are approximately four times higher than those from sum-

mer. Possible reasons for this seasonal difference are changes in vehicular emissions caused by cold starts during cooler parts of the year or increased residential heating and burning, or the slower oxidation of intermediate volatility compounds to condensable species.

For the rural locations, the hourly averages of CPC concentrations are 3690±2630 1/cm$^3$ (max: 41 200; min: 977 1/cm$^3$) and 3880±2200 1/cm$^3$ (max: 28 470; min: 1050 1/cm$^3$) for WFM02 and PSP04, respectively. The largest particle number concentrations occur mainly in the ultrafine particle sizes and are associated with occasional daytime particle growth events (Zhang et al., 2005). The binned size distributions shown in the inset Fig. 5 for each site show that the highest fraction of the total number concentration measured at the QC site is in the smallest size bin (8.35–19.8 nm), while the WFM and PSP aerosol size distributions are characterized by maxima in the largest size bin (67.3–283.9 nm). This difference can be attributed to occurrence of small fresh particles by primary emission for the QC campaigns and an enhancement of coagulation and condensation processes in aged air for the WFM02 and PSP04 campaigns.

### 3.7 Time series size distributions, particle concentrations, and $PM_{2.5}$ mass

Figures 6–9 present complete time series traces for SMPS size distributions, CPC number concentrations, and $PM_{2.5}$ mass concentrations by the Tapered Element Oscillating Microbalance (TEOM) (Schwab et al., 2006) during the four measurement campaigns (summertime for the QC01 campaign, wintertime for the QC04 campaign, summertime for the WFM02 campaign, and summertime for the PSP04 campaign). These time series plots provide insights into the range in particle size distributions, number concentrations, and $PM_{2.5}$ mass concentrations (colored by approximate ion balance). The amounts of data available for each measurement allow initial validations between the Nano SMPS and LDMA SMPS and SMPS and CPC and a more detailed inspection of the data sets. Data was flagged and removed from the analysis if any of the following conditions was known to apply: 1) when less than 75% of the data is avail-

able for an hour; 2) when an instrument was malfunctioning; or 3) when the data is an outlier based on statistical analysis. Data completeness is about 95%, 97%, 66%, 95% measured by SMPS (8.35–283.9 nm combined by Nano SMPS and LDMA SMPS) for the QC01, WFM02, QC04, and PSP04 campaigns, respectively. Lower data completeness for the QC04 campaign is mainly due to malfunctioning of LDMA SMPS in the early of sampling period (10–14 January) and malfunction of Nano SMPS in the middle of sampling period (24–26 January).

As with the insets of the previous Fig. 5, in addition to the total number concentration measured by the CPC, the number concentrations by SMPS have been binned into four consecutive ranges (8.35–19.8, 21.3–37.9, 40.7–62.6, 67.3–283.9 nm) based on the dynamics of number concentrations. The range of 8.35–19.8 nm corresponds to the initial growth period with or after particle nucleation. The ranges of 21.3–37.9 nm and 40.7–62.6 nm corresponds to consecutive growth or emissions, so called "ultrafine mode" ($D_m$=10–100 nm, $D_m(=D_p)$; mobility particle diameter from SMPS), and the range of 67.3–283.9 nm corresponds to the longer lived accumulation mode particles. The size distributions of number concentrations are well known to be quite dynamic, and the color contour plots clearly show that is indeed the case for these measurements.

### 3.8 Particle size distributions in the urban areas

The contour plots in Figs. 6 and 7 provide an overview of the evolution of the temporal particle size distributions and the time series line graphs show particle concentrations measured by the CPC and SMPS (summed over the size range of 8.35–283.9 nm). The upper time series line graph is $PM_{2.5}$ mass concentrations, colored by the major ion charge balance for the QC01 and QC04 campaigns. As seen from the graph panel showing binned number concentrations from SMPS, the majority of the measured particles reside in the "ultrafine mode" ($D_m$=10–100 nm) for the urban locations.

The contour plots from Figs. 6 and 7 show the concentration of particles in each size bin (in $dN/d\log D_m$ (1/cm$^3$)). The logarithmic vertical axis is the particle diameter ($D_m$),

and horizontal axis is the time during a sampling period. The particle number concentrations are shown by the color with highest concentrations being the hottest color. The characteristic feature of both QC01 and QC04 data sets is a daily diurnal pattern in a form of a gradual increase from the early morning and a decrease in late morning, consistent with vehicle emissions particle sources. The high particle concentration events are consistently associated with the morning traffic. The mean particle size during these events is between 8.35 to 19.8 nm for the QC01 campaign and between 8.35 to 37.9 nm for the QC04 campaign. The size range of 8.35–19.8 nm accounts for about 45% in total number concentrations measured by the SMPS (8.35–283.9 nm) for the QC01 campaign and about 54% for the QC04 campaign. There is a strong association between CPC and the SMPS size range of 8.35–19.8 nm, yielding $r^2$ values of 0.56 and 0.72 for the QC01 and QC04 campaigns, respectively. The morning rush hour traffic occurs prior to the lifting of the nighttime inversion and remains near the boundary layer sampled by these measurements. The evening rush hour is not readily discernable, due at least in part to the expanded boundary layer later in the day. The Figs. 6 and 7 show that there is no statistically discernable relationship in measured size ranges between weekdays (Monday to Friday) and weekends (Saturday to Sunday) for the QC01 and QC04 campaigns.

Figures 6 and 7 also show time series traces for the hourly number concentration ($1/cm^3$) measured by the CPC. The number concentrations of "combined SMPS" (8.35–283.9 nm) and the CPC track each other well during periods of low concentrations and during traffic activities. Linear regression slopes for the above between these two parameters result in correlations slopes of 0.76 and 1.04 (forced to zero) and $r^2$ values of 0.59 and 0.90 as shown in Fig. 4.

As noted above, the molar ion balance of the major inorganic ions ($[NH_4^+] - 2\times[SO_4^{2-}] - [NO_3^-]$) from Q-AMS measurements (Bae et al., 2007; Drewnick et al., 2004) was calculated and used as an indicator of the degree of neutralization of the aerosol (acidic particles are characterized by an ion balance value of less than zero). During summertime for the QC01 campaign, the Q-AMS reported nitrate concentrations were much

lower than during the winter campaign, which is consistent with the thermodynamic hypothesis that nitrate concentrations in summertime ambient particles is usually very low because of displacement of $HNO_3$. During wintertime for the QC04 campaign, the particles are closer to neutral, on average, with more nitrate and less sulfate. This is consistent with the lower oxidation rates expected in the winter. Specifically, during the summer campaign, $PM_{2.5}$ mass concentrations tend to be higher during periods that the particles are most acidic. This association is not observed for the winter campaign. In contrast to the $PM_{2.5}$ mass, there is no statistical significance when comparing ion balance with the number concentrations which has low $r^2$ of 0.00 and 0.01 from QC01 and QC04, respectively. It suggests that ion balance is independent of both the particle number concentrations and their production in the New York City urban area.

### 3.9 Particle size distributions in the rural areas

Figures 8 and 9 show an overview of the evolution of the temporal particle size distributions, and particle concentrations and $PM_{2.5}$ mass concentrations for the WFM02 and PSP04 campaigns. The binned particle concentrations from the SMPS for the WFM02 and PSP04 campaigns show very different distributions than observed in New York City. While the particles are in all size ranges ("nucleation mode" ($D_m$=<10 nm), "ultrafine mode" ($D_m$=10–100 nm) and "accumulation mode" ($D_m$=> 100 nm)), the largest fraction of particles in the rural campaigns was found in the size range of 67.3–283.9 nm (about 40% of the total number concentrations for the WFM02 campaign and about 46% for the PSP04 campaign).

Evident in the color contour plots of Figs. 8 and 9 for both sites is one or more particle growth events, with high particle concentrations down to the lowest particle diameters. The two strongest growth events occurred on 24 July (Wednesday) for the WFM02 campaign and, same date but different year, on 24 July (Saturday) for the PSP04 campaign, in each case beginning in the early to mid-morning time and extending through the afternoon and evening into the next day. These strong particle growth events will be investigated in relation to physical and chemical driving forces in

a companion study.

Excluding these particle growth days, no distinguishable daily diurnal pattern has been observed in the signals from either rural area. In addition, there is no statistically discernable relationship in measured size ranges between weekdays and weekends for the WFM02 and PSP04 campaigns without the particle growth days. The number concentrations between the combined SMPS [8.35–283.9 nm] and the CPC track each other well during periods of low concentrations as well as particle growth events with linear regression slopes of 1.13–1.06 (forced to zero) and $r^2$ of 0.96–0.97 (Fig. 4).

As with the New York City campaigns, the major ion balance ($[NH_4^+] - 2\times[SO_4^{2-}] - [NO_3^-]$) has been used to color the $PM_{2.5}$ mass concentration time series. $NH_4^+$ and $SO_4^{2-}$ data were taken from the AMS measurement, but in this case the $NO_3^-$ data were taken from the PILS measurement due to interference of organic signals in AMS nitrate measurements (Bea et al., 2007). Of the periods of elevated $PM_{2.5}$ mass concentration during these two campaigns, most periods show significantly negative (acidic) ion balance – as would be expected from the sulfate dominated northeast. In contrast, there is no statistical significance in the association between ion balance and particle number concentrations with low $r^2$ of 0.02 and 0.01 for WFM02 and PSP04, respectively.

### 3.10 Relationship between $PM_{2.5}$ mass and particle size diameter

Figure 10 presents time series of the median particle size diameter (nm), and the 5th and 95th percentile diameters colored as a function of the $PM_{2.5}$ mass concentrations. The higher mass concentrations were measured simultaneously with the higher particle diameters; and as we have seen, mass concentrations are generally anti-correlated with number concentrations. These observations can be explained by considering two limiting cases. The small particle limit is generally accompanied by observations of low $PM_{2.5}$ mass, high number concentration, and low diameter caused by the occurrence of "small fresh particles" associated with two possible processes; 1) recent primary emission (as observed for the QC01 and QC04 campaigns) associated with Black Car-

bon (BC) or hydrocarbon-like organic aerosol (HOA), 2) particle nucleation and growth associated with sulfuric acid by sulfur dioxide and sulfate (Jung et al., 2006) (as observed for the WFM02 and PSP04 campaigns). The large particle limit is accompanied by observation of high $PM_{2.5}$ mass, lower number concentration, and higher diameter. These episodes are mainly due to an enhancement of coagulation and condensation processes in relatively "aged air". These observations have also important implications, from a technical point of view, for urban/rural air quality monitoring. Specifically, number concentrations and $PM_{2.5}$ mass exhibit some properties which are complementary for monitoring the urban/rural air quality. Number concentration is highly sensitive to the fresh vehicle exhaust emissions of ultrafine particles, whereas $PM_{2.5}$ mass is highly influenced by the aged aerosol linked to the urban background mostly occurring in the accumulation mode due to the atmospheric processing of vehicle emissions and other sources.

### 3.11 Relationship between $PM_{2.5}$ mass and condensation sink (CS)

In order to understand the dynamic effects of aerosol growth for the QC 01, WFM02, QC 04 and PSP04 campaigns, the condensation sink (CS) was calculated as described earlier. Dal Maso et al. (2002) observed values for the CS of $4–7\times10^{-3}\,s^{-1}$ in the rural (forest) area and $2\times10^{-3}\,s^{-1}$ under coastal conditions. Kulmala et al. (2005) presented that the values of the CS between $1.3\times10^{-2}$ and $0.6\times10^{-4}\,s^{-1}$ in variety locations. The CS was usually higher in more polluted areas ($5–7\times10^{-2}\,s^{-1}$) encountered in New Delhi, while Athens and Marseille CS in the European cities was 5–10 times lower. Leskinen et al. (2008) also showed values of $1.4–13\times10^{-3}\,s^{-1}$ in a smog chamber study.

The averages (±standard deviation) of the CS (8.35–283.9 nm) yielded $1.6(\pm0.7)\times10^{-2}$, $6.5(\pm3.3)\times10^{-3}$, $2.4(\pm0.9)\times10^{-2}$, and $6.9(\pm3.5)\times10^{-3}$ for the QC 01, WFM02, QC 04 and PSP04 campaigns, respectively. The CS in the urban areas is roughly two to three times higher than rural areas due to differences in number concentrations and size distributions.

Figure 11 presents evolutions of particle size distributions and CS (1/s), time series traces for the hourly $PM_{2.5}$ mass concentrations ($\mu g/cm^3$). The right panels of Fig. 11 show the pairwise correlation scatterplots between $PM_{2.5}$ mass and CS for the four campaigns. There are markedly different relationships between the urban and rural locations. While the good relationship ($r^2$>0.5) between $PM_{2.5}$ mass and CS in the urban areas, there is a less clear association with low $r^2$ of 0.24 and 0.22 for the WFM02 and PSP04 campaigns, respectively. The stronger relationship between $PM_{2.5}$ mass and CS in the urban areas can be explained by the large contribution to $PM_{2.5}$ mass by dynamic condensation processes from primary particles for the urban site. For the rural areas, the scatterplots indicate a more complicated picture. The two strongest growth events produce relatively high CS values without large $PM_{2.5}$ mass, but other data periods show poor association between CS and $PM_{2.5}$ mass.

## 4 Summary and conclusions

This study presents measurements of particle number concentrations and size distributions using combined data from a Nano SMPS and an LDMA SMPS. Measurements were conducted at the sites of Whiteface Mountain (WFM, summer 2002) and Pinnacle State Park (PSP, summer 2004) in rural areas of New York State and at the urban site of Queens College (QC) in New York City in summer 2001 and winter 2004.

We have analyzed the size distributions with and without corrections for the diffusion losses of particles, both in the inlet sampling lines, and in the SMPS systems. We showed that inclusion of these corrections is important for nano particle concentration and size distribution measurements. The diffusion correction uncovers a nano particle mode between 10 and 15 nm mobility diameter which is not present in the uncorrected data for the measurements in New York City. Slopes of scatterplots between the total number concentrations measured by a stand alone CPC and the integrated total number concentration from the combined SMPS measurements range from 0.76 to 1.13, and $r^2$ values for three of the four campaigns are 0.90 or above (the $r^2$ value for the

fourth campaign is 0.59).

The New York City measurements show a daily pattern of high total number concentrations in the morning hours associated with the morning rush hour and traffic emissions. Winter concentrations average about four times greater than summer concentrations at the Queens site. The rural sites have average summer concentrations that are about a factor of 5-6 lower than the Queens summer concentrations. The rural summer size distributions have much larger mode sizes, with largest concentrations in the accumulation mode.

Low $PM_{2.5}$ mass quite often is associated with high number concentration and low diameter in our observations. These associations are caused by the occurrence of small fresh particles associated with primary emission (for the QC01 and QC04 campaigns), or by fresh particle nucleation and growth (for the WFM02 and PSP04 campaigns). In contrast, the observations of high $PM_{2.5}$ mass, is often associated with lower number concentration and larger diameter, which we believe indicate an enhancement of coagulation and condensation processes in photochemically aged air. There are markedly different values for the calculated condensation sink between the urban and rural locations, with campaign averages between 0.006–0.007 $s^{-1}$ for the rural sites, and 0.016–0.024 $s^{-1}$ for the urban site. The condensation sink has a strong association with $PM_{2.5}$ mass for the New York City site, but a much weaker relation with $PM_{2.5}$ mass at the rural sites.

*Acknowledgements.* This work was supported by NOAA award number NA05OAR4310105, by the New York State Energy Research and Development Authority (NYSERDA) contracts 4918ERTERES99, 5060ERTERER99, and 6183; and by EPA cooperative agreement #R828060010; and New York State Department of Environmental Conservation (NYSDEC) contract #C004210. Although the research described in this article has been funded in part by EPA, it has not been subjected to the agency's required peer and policy review and, therefore, does not necessarily reflect the views of the agency and no official endorsement should be inferred. Helpful discussion and the assistance of ASRC scientists Qi Zhang, John Spice, Fangqun Yu, Silke Weimer in EMPA, Dirk Felton in DEC are gratefully acknowledged.

## References


Brockman, J. E.: Sampling and transport of aerosols, in: Aerosol Measurement: Principles, Techniques, and Applications, 2nd edn., edited by: Baron, P. A. and Willeke, K., John Wiley and Sons, New Jersey, 2001.

Bae, M.-S., Schwab, J. J., Zhang, Q., Hogrefe, O., Demerjian, K. L., Weimer, S., Rhoads, K., Orsini, D., Venkatachari, P., and Hopke, P. K.: Interference of organic signals in highly-time resolved nitrate measurements by aerosol mass spectrometer, J. Geophys. Res., 112, D22305, doi:10.1029/2007JD008614, 2007.

Buonanno, G., Lall, A. A., and Stabile, L.: Temporal size distribution and concentration of particles near a major highway, Atmos. Environ., 43, 1100–1105, 2009.

Chow, J. C., Watson, J. G., Savage, N., Solomon, C. J., Cheng, Y.-S., McMurry, P. H., Corey, L. M., Bruce, G. M., Pleus, R. C., Biswas, P., and Wu, C.-Y.: Nanoparticles and the environment, J. Air Waste Manage., 55, 1411–1417, 2005.

Dal Maso, M., Kulmala, M., Lehtinen, K. E. J., Mäkelä, J. M., Aalto, P., and O'Dowd, C. D.: Condensation and coagulation sinks and formation of nucleation mode particles in coastal and boreal forest boundary layers, J. Geophys. Res., 107, 8097, doi:10.1029/2001JD001053, 2002.

Dal Maso, M., Kulmala, M., Riipinen, I., Wagner, R., Hussein, T., Aalto, P. P., and Lehtinen, K. E. J.: Formation and growth of fresh atmospheric aerosols: eight years of aerosol size distribution data from SMEAR II, Hyytiälä, Finland, Boreal Environ. Res., 10, 323–336, 2005.

Dall'Osto, M., Booth, M. J., Smith, W., Fisher, R., and Harrison, R. M.: A study of the size distributions and the chemical characterization of airborne particles in the vicinity of a large integrated steelworks, Aerosol Sci. Tech., 42, 981–991, 2008.

Drewnick, F., Schwab, J. J., Jayne, J. T., Canagaratna, M., Worsnop, D. R., and Demerian, K. L.: Measurement of ambient aerosol composition during the PMTACS-NY 2001 using an aerosol mass spectrometer. Part 1: mass concentrations, Aerosol Sci. Tech., 38, 92–103, 2004.

Frank, B. P., Saltiel, S., Hogrefe, O., Grygas, J., and Garland Lala, G.: Determination of mean particle size using the electrical aerosol detector and the condensation particle counter: comparison with the scanning mobility particle sizer, J. Aerosol Sci., 39, 19–29, 2008.

Fuchs, N. A. and Sutugin, A. G.: Highly dispersed aerosol, in: Topics in Current Aerosol Research, edited by: Hidy, G. M. and Brock, J. R., Pergamon, New York, 1–60, 1971.

Hanson, D. R. and Eisele, F.: Diffusion of $H_2SO_4$ in humidified nitrogen: hydrated $H_2SO_4$, J. Phys. Chem. A, 104, 1715–1719, 2000.
Hinds, W. C.: Aerosol Technology: Properties, Behavior, and Measurement of Airborne Particles, John Wiley and Sons, New Jersey, 1982.
Hopke, P. K.: Contemporary threats and air pollution, Atmos. Environ., 43, 87–93, 2009.
Jeong, C.-H. and Evans, G. J.: Inter-comparison of a fast mobility particle sizer and a scanning mobility particle sizer incorporating an ultrafine water-based condensation particle counter, Aerosol Sci. Tech., 43, 364–373, 2009.
Jeong, C.-H., Hopke, P. K., Chalupa, D., and Utell, M.: Characteristics of nucleation and growth events of ultrafine particles measured in Rochester, NY, Environ. Sci. Technol., 38, 1933–1940, 2004.
Jung, J., Adams, P. J., and Pandis, S. N.: Simulating the size distribution and chemical composition of ultrafine particles during nucleation events, Atmos. Environ., 40, 2248–2259, 2006.
Kulmala, M., Laakso, L., Lehtinen, K. E. J., Riipinen, I., Dal Maso, M., Anttila, T., Kerminen, V.-M., Hõrrak, U., Vana, M., and Tammet, H.: Initial steps of aerosol growth, Atmos. Chem. Phys., 4, 2553–2560, 2004a, http://www.atmos-chem-phys.net/4/2553/2004/.
Kulmala, M., Petäjä, T., Mnkknen, P., Koponen, I. K., Dal Maso, M., Aalto, P. P., Lehtinen, K. E. J., and Kerminen, V.-M.: On the growth of nucleation mode particles: source rates of condensable vapor in polluted and clean environments, Atmos. Chem. Phys., 5, 409–416, 2005, http://www.atmos-chem-phys.net/5/409/2005/.
Kulmala, M., Vehkamaki, H., Petaja, T., Dal Maso, M., Lauri, A., Kerminen, V.-M., Birmili, W., and McMurry, P. H.: Formation and growth rates of ultrafine atmospheric particles: a review of observations, J. Aerosol Sci., 35, 143–176, 2004b.
Lehtinen, K. E. J., Korhonen, H., Dal Maso, M., and Kulmala, M.: On the concept of condensation sink diameter, Boreal Environ. Res., 8, 405–411, 2003.
Leskinen, A. P., Kulmala, M., and Lehtinen, K. E. J.: Growth of nucleation mode particles: source rates of condensable vapour in a smog chamber, Atmos. Environ., 42, 7405–7411, 2008.
McMurry, P. H., Litchy, M., Huang, P.-F., Cai, X., Turpin, B. J., Dick, W. D., and Hanson, A.: Elemental composition and morphology of individual particles separated by size and hygroscopicity with the TDMA, Atmos. Environ., 30, 101–108, 1996.

McMurry, P. H.: A review of atmospheric aerosol measurements, Atmos. Environ., 34, 1959–1999, 2000.
Paul, M. W., Aron, V., Paul, E. W., Markku, K., Kari, E. J. L., and Timo, V.: Mass and thermal accommodation during gas-liquid condensation of water, Phys. Rev. Lett., 93, 075701, doi:10.1103/PhysRevLett.93.075701, 2004.
Pirjola, L., Kulmala, M., Wilck, M., Bischoff, A., Stratmann, F., and Otto, E.: Formation of sulphuric acid aerosols and cloud condensation nuclei: an expression for significant nucleation and model comprarison, J. Aerosol Sci., 30, 1079–1094, 1999.
Qian, S., Sakurai, H., and McMurry, P. H.: Characteristics of regional nucleation events in urban East St. Louis, Atmos. Environ., 41, 4119–4127, 2007.
Reineking, A. and Porstendörfer, J.: Measurements of particle loss functions in a differential mobility analyzer (TSI, Model 3071) for different flow rates, Aerosol Sci. Tech., 483–486, 5, 1986.
Rodrigue, J., Ranjan, M., Hopke, P. K., and Dhaniyala, S.: Performance comparison of scanning electrical mobility spectrometers, Aerosol Sci. Tech., 41, 360–368, 2007.
Schwab, J. J., Felton, H. D., and Demerian, K. L.: Aerosol chemical composition in New York State from integfated filter samples: urban/rural and seasonal contrasts, J. Geophys. Res., 109, D16S05, doi:10.1029/2003JD004078, 2004.
Schwab, J. J., Felton, H. D., Rattigan, O. V., and Demerian, K. L.: New York State urban and rural measurements of continuous $PM_{2.5}$ mass by FDMS, TEOM, and BAM, J. Air Waste Manage., 56, 372–383, 2006.
Stanier, C. O., Khlystov, A. Y., and Pandis, S. N.: Nucleation events during the Pittsburgh air quality study: description and relation to key meteorological, gas phase, and aerosol parameters, Aerosol Sci. Tech., 38, 253–264, 2004.
Su, W.-C., Wu, J., Marijnissen, J. C. M., and Cheng, Y. S.: Deposition of man-made fibers in a human nasal airway, Aerosol Sci. Tech., 42, 173–181, 2008.
TSI, Inc.: Scanning Mobility Particle Sizer (SMPS) spectrometer diffusion loss correction, Application Note SMPS-001, Shoreview, MN, 2006.
Wang, J., Flagan, R. C., and Seinfeld, J. H.: Diffusional losses in particle sampling systems containing bends and elbows, J. Aerosol Sci., 33, 843–857, 2002.
Watson, J. G., Chow, J. C., Park, K., and Lowenthal, D. H.: Nanoparticle and ultrafine particle events at the Fresno supersite, J. Air Waste Manage., 56, 417–430, 2006.
Willeke, K.: Temperature dependence of particle slip in a gaseous medium, J. Aerosol Sci., 7,

381–387, 1976.
Zhang, Q., Canagaratna, M., Jayne, J. T., Worsnop, D. R., and Jimenez, J.-L.: Time- and size-resolved chemical composition of submicron particles in Pittsburgh: implications for aerosol sources and processes, J. Geophys. Res., 110, D07S09, doi:10.1029/2004JD004649, 2005.
Zhang, R., Suh, I., Zhao, J., Zhang, D., Fortner, E. C., Tie, X., Molina, L. T., and Molina, M. J.: Atmospheric new particle formation enhanced by organic acids, Science, 304, 1487–1490, 2004.

**Table 1.** Operation parameters for the particle sizing and counting instruments.

| QC 01 | CPC 3022 | Nano SMPS | Long-tube SMPS |
|---|---|---|---|
| Operator | ASRC | DEC | ASRC |
| Cycle length, min | 5 min | 2.5 | 5 (2 scans of 2.5 min) |
| Inlet sample flow, l/min | 0.3, 1.5 | 0.3 | 0.3, 0.6, 1.0 |
| Sheath flow, l/min | N/A | 3 | 3.0, 6.0, 10.0 |
| Neutralizer Strength | N/A | 2 mCi | 2 mCi |
| CPC Model | 3022 | 3025 | CPC3010, CPC3025 |
| Diameter range, nm | 50% at 7 nm 90% at 15 nm | 4.7–160 | Varied |
| Number of Bins | N/A | 50 | Varied |
| *D* (lower bound–upper bound) | N/A | 4.53–165.57 | Varied |
| **WFM 02** | **CPC 3022** | **Nano SMPS** | **Long-tube SMPS** |
| Operator | ASRC | ASRC | ASRC |
| Cycle length, min | 10 s | 5 (2 scans of 2.5 min) | 5 (2 scans of 2.5 min) |
| Inlet sample flow, l/min | 1.5 | 0.6+5.0 bypass | 0.6 |
| Sheath flow, l/min | N/A | 6 | 6 |
| CPC Model | 3022 | 3025 | 3010 |
| Neutralizer Strength | N/A | 2 mCi | 2 mCi |
| Diameter range, nm | 50% at 7 nm 90% at 15 nm | 3.28–104 | 10.4–407 |
| Number of Bins | N/A | 49 | 52 |
| *D* (lower bound–upper bound) | N/A | 3.16–107.52 | 10.03–423.07 |
| **QC 04** | **CPC 3022** | **Nano SMPS** | **Long-tube SMPS** |
| Operator | ASRC | DEC | ASRC |
| Cycle length, min | 5 min | 2.5 | 5 (2 scans of 2.5 min) |
| Inlet sample flow, l/min | 1.5 | 0.6 | 0.3 |
| Sheath flow, l/min | N/A | 6 | 3 |
| CPC Model | 3022 | 3025 | 3010 |
| Neutralizer Strength | N/A | 2 mCi | 2 mCi |
| Diameter range, nm | 50% at 7 nm 90% at 15 nm | 3.28–104 | 16–626 |
| Number of Bins | N/A | 49 | 52 |
| *D* (lower bound–upper bound) | N/A | 3.16–107.52 | 15.43–650.87 |
| **PSP 04** | **CPC 3022** | **Nano SMPS** | **Long-tube SMPS** |
| Operator | ASRC | ASRC | ASRC |
| Cycle length, min | 5 min | 5 (2 scans of 2.5 min) | 5 (2 scans of 2.5 min) |
| Inlet sample flow, l/min | 1.5 | 0.3 | 0.3 |
| Sheath flow, l/min | N/A | 3 | 3 |
| CPC Model | 3022 | 3025 | 3010 |
| Neutralizer Strength | N/A | 2 mCi | 2 mCi |
| Diameter range, nm | 50% at 7 nm 90% at 15 nm | 4.7–149 | 16–626 |
| Number of Bins | N/A | 49 | 52 |
| *D* (lower bound–upper bound) | N/A | 4.53–154.07 | 15.43–650.87 |

**Table 2.** Sum of number concentration ($1/cm^3$) in size range for empirical transfer function for the Nano SMPS.

| | 1st Analysis Period | | | | 2nd Analysis Period | | | |
|---|---|---|---|---|---|---|---|---|
| Size Range (nm) | QC01 | WFM02 | QC04 | PSP04 | QC01 | WFM02 | QC04 | PSP04 |
| 8.35–19.8 | 7753 | 1054 | 23604 | 278 | 3343 | 149 | 28671 | 310 |
| 21.3–37.9 | 2272 | 1425 | 19167 | 871 | 2469 | 532 | 18391 | 725 |
| 40.7–62.6 | 1364 | 866 | 6501 | 555 | 2216 | 860 | 8026 | 688 |
| 67.3–96.5 | 1541 | 471 | 2165 | 336 | 1956 | 871 | 2829 | 419 |
| Number of raw data points | 10 | 10 | 10 | 10 | 10 | 10 | 10 | 10 |
| Data from | 0:52:01 | 7:30:00 | 1:41:46 | 1:40:01 | 2:16:11 | 1:40:00 | 3:47:43 | 4:10:01 |
| Data to | 1:14:39 | 8:15:00 | 2:04:28 | 2:25:01 | 2:40:22 | 2:25:01 | 4:10:26 | 4:55:01 |
| on | 4 Jul 2001 | 16 Jul 2002 | 11 Jan 2004 | 31 Jul 2004 | 17 Jul 2001 | 31 Jul 2002 | 11 Jan 2004 | 31 Jul 2004 |

**Table 3.** Upper and lower limit at the merge size points.

| (Unit; nm) | | QC 01[(1)] | WFM 02[(1)] | QC 04[(1)] | PSP 04[(2)] |
|---|---|---|---|---|---|
| Nano SMPS | Upper Limit | 64.98 | 64.98 | 64.98 | 39.26 |
| | Lower Limit | 60.46 | 60.46 | 60.46 | 36.54 |
| LDMA SMPS | Upper Limit | 64.91 | 65.15 | 65.09 | 39.33 |
| | Lower Limit | 60.40 | 60.63 | 60.57 | 36.60 |

[(1)] Merge size point: 62.6
[(2)] Merge size point: 37.9

**Table 4.** Statistical characteristics of hourly averaged number concentrations measured by CPC and SMPS with diffusion loss corrections.

| SITE | Statistical Value | CPC | 8.35–283.9 nm | 8.35–19.8 | 21.3–37.9 | 40.7–62.6 | 67.3–283.9 |
|---|---|---|---|---|---|---|---|
| QC 01 | Valid (hr) | 759 | 773 | 773 | 773 | 773 | 773 |
| | Mean | **22 124** | **24 122** | **10 871** | **6030** | **3355** | **3867** |
| | Median | 19 845 | 22 022 | 9633 | 4928 | 3002 | 3643 |
| | Std. Deviation | 10 701 | 10 668 | 5998 | 4036 | 1897 | 1819 |
| | Minimum | 4524 | 5185 | 2058 | 635 | 460 | 778 |
| | Maximum | 77 056 | 69 324 | 42 149 | 29 358 | 12 550 | 9543 |
| WFM 02 | Valid | 568 | 659 | 659 | 659 | 659 | 659 |
| | Mean | **3691** | **4106** | **603** | **916** | **956** | **1631** |
| | Median | 3122 | 3237 | 225 | 542 | 608 | 1490 |
| | Std. Deviation | 2626 | 3231 | 1879 | 1186 | 909 | 981 |
| | Minimum | 977 | 978 | 4 | 42 | 65 | 143 |
| | Maximum | 41 218 | 47 685 | 39 281 | 9659 | 5522 | 5385 |
| QC 04 | Valid | 650 | 431 | 431 | 431 | 431 | 431 |
| | Mean | **87 574** | **66 760** | **35 932** | **19 516** | **7654** | **3658** |
| | Median | 84 612 | 63 058 | 32 015 | 18 021 | 6843 | 3120 |
| | Std. Deviation | 26 875 | 22 579 | 14 464 | 7526 | 3500 | 1985 |
| | Minimum | 38 290 | 27 085 | 12 282 | 6813 | 1534 | 777 |
| | Maximum | 269 160 | 163 164 | 89 978 | 49 972 | 20 993 | 12 898 |
| PSP 04 | Valid | 587 | 564 | 564 | 564 | 564 | 564 |
| | Mean | **3881** | **4052** | **520** | **690** | **980** | **1862** |
| | Median | 3269 | 3450 | 277 | 422 | 726 | 1657 |
| | Std. Deviation | 2201 | 2619 | 1078 | 983 | 813 | 1089 |
| | Minimum | 1053 | 858 | 4 | 35 | 131 | 93 |
| | Maximum | 28 471 | 33 380 | 17 489 | 13 472 | 5522 | 5881 |

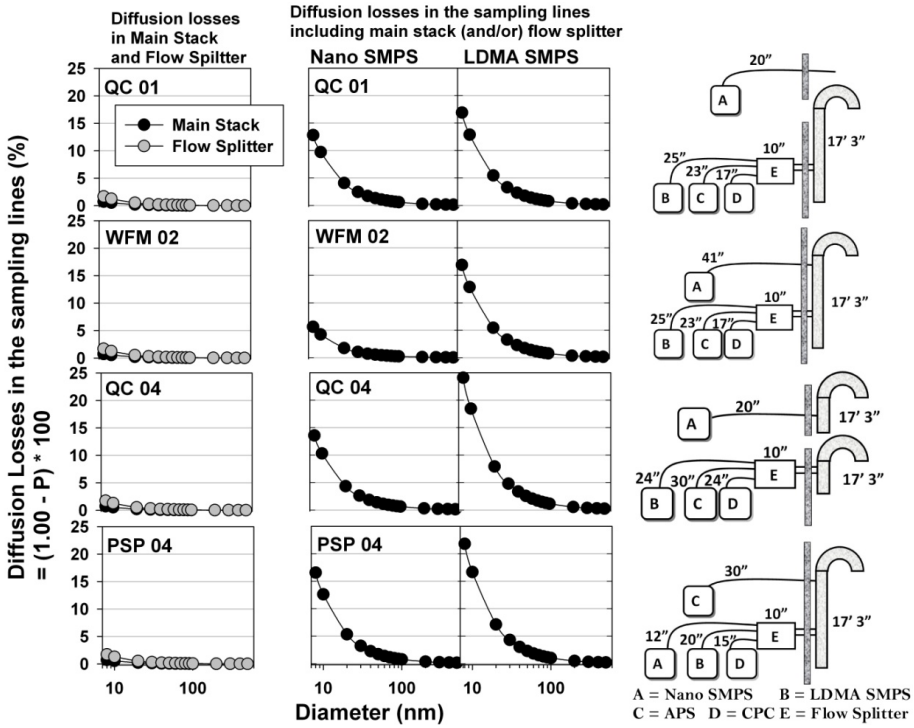


**Fig. 1.** Computed diffusion losses (%) for the Nano and LDMA SMPS sampling lines. The left panels only show the diffusion losses in main stack and flow splitter. The center panels show the diffusion losses in the sampling lines including main stack (and/or) flow splitter. The right panels show the schematic diagrams for the setup related to campaigns (note: total flow rate of Nano SMPS for the WFM campaign includes 5.0 lpm bypass).

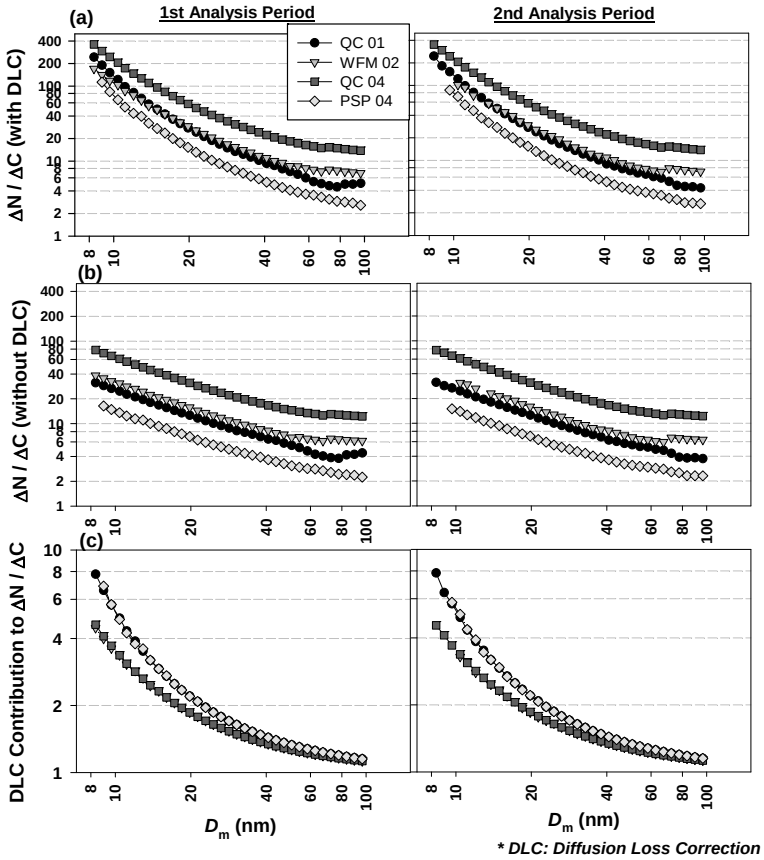


**Fig. 2.** Empirical transfer function (defined as $\Delta N/\Delta C$) for the Nano SMPS in each of the four measurement campaigns. Panel **(a)** shows $\Delta N/\Delta C$ with the diffusion loss correction included, panel **(b)** shows $\Delta N/\Delta C$ without the diffusion loss correction, and panel **(c)** shows the contribution of the diffusion loss correction to $\Delta N/\Delta C$.

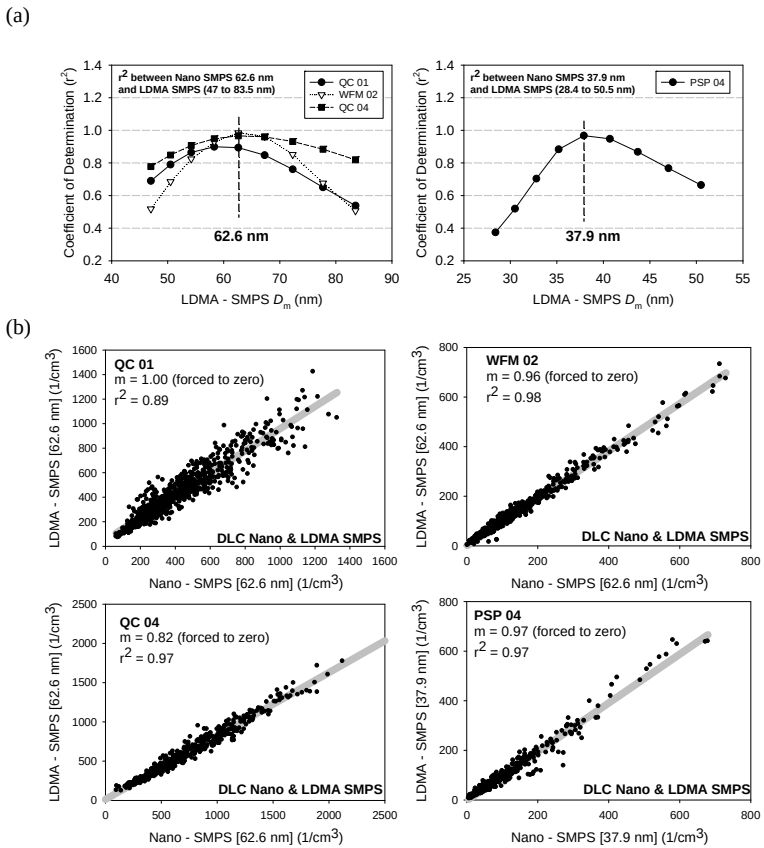


**Fig. 3.** Comparison of **(a)** correlation coefficient between Nano SMPS and LDMA SMPS at the QC01, WFM02, QC04, and PSP04 campaigns, **(b)** hourly averaged LDMA SMPS (62.6 nm) and Nano SMPS (62.6 nm) at the QC01, WFM02, and QC04 campaigns, respectively, hourly averaged LDMA SMPS (37.9 nm) and Nano SMPS (37.9 nm) at the PSP04 campaigns.

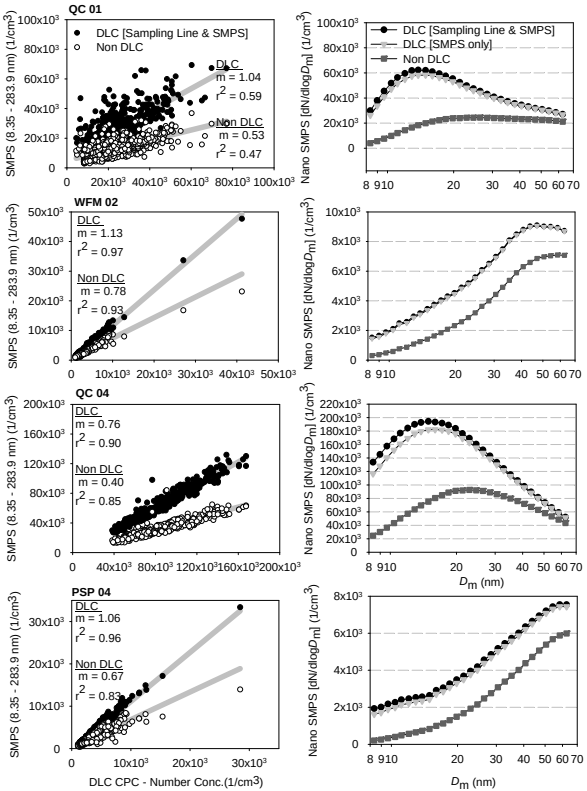


**Fig. 4.** Pairwise correlation scatterplots between hourly averaged diffusion loss corrected-DLC CPC and hourly averaged SMPS (8.35–283.9 nm) with number concentrations ($1/\mathrm{cm}^3$) corrected for diffusion loss (solid circles) and not corrected for diffusion loss (open circles), and Nano SMPS average size distributions ($\mathrm{dN/dlog}D_\mathrm{m}$) ($1/\mathrm{cm}^3$) corrected for diffusion loss (solid circles) and not corrected for diffusion loss (open circles) for the QC01, WFM02, QC04, and PSP04 campaigns. (Note: CPC is assumed to have the same size distribution as Nano SMPS for diffusion loss correction.)

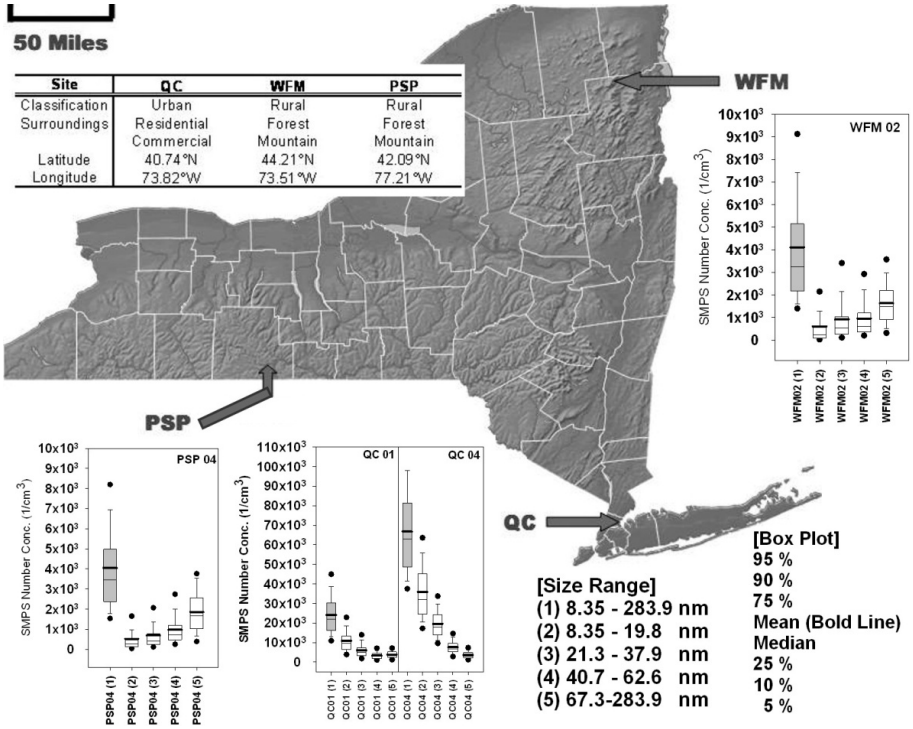


**Fig. 5.** Location of sampling sites and number concentrations by SMPS from Pinnacle State Park (PSP), Whiteface Mountain (WFM) and Queens College (QC) in New York. (The bold line inside the box is the mean value; the boundary of the box closest to zero is the 25th percentile; the thin line inside the box is the median and the boundary of the box farthest from zero is the 75th percentile. Whiskers correspond to the 10th and 90th percentiles. Upper and lower closed dots correspond to the 5th and 95th percentiles.)

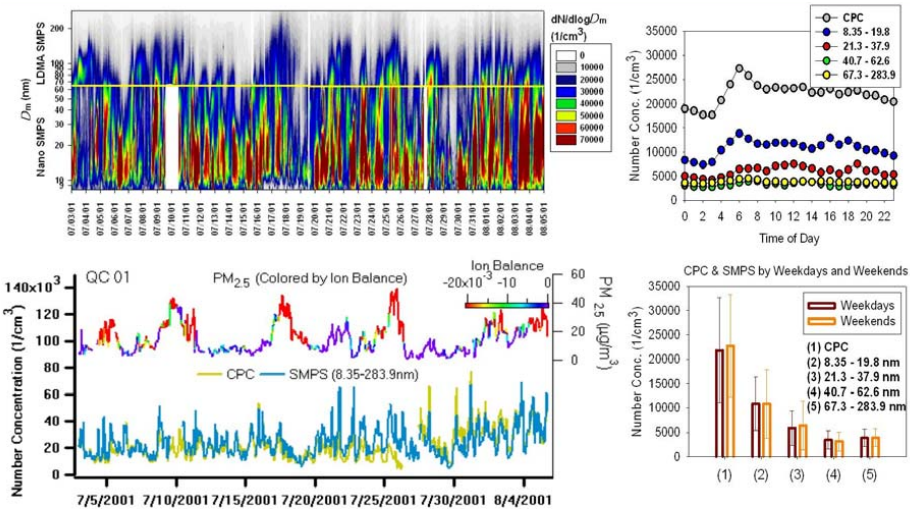


**Fig. 6.** Evolution of particle size distributions and particle concentrations (dN/dlog$D_m$) (1/cm$^3$), time series traces for the hourly number concentration (1/cm$^3$) measured by the CPC (dark yellow line) and SMPS (8.35–283.9 nm) (dark blue line), as well as $PM_{2.5}$ mass concentrations (colored by the ion charge balance), hour-of-day series by CPC (gray) and SMPS (8.35–19.8 nm: blue, 21.3–37.9: red, 40.7–62.6: green, 67.3–283.9: yellow) and weekdays (brown) and weekends (orange) in number concentrations for the QC01.

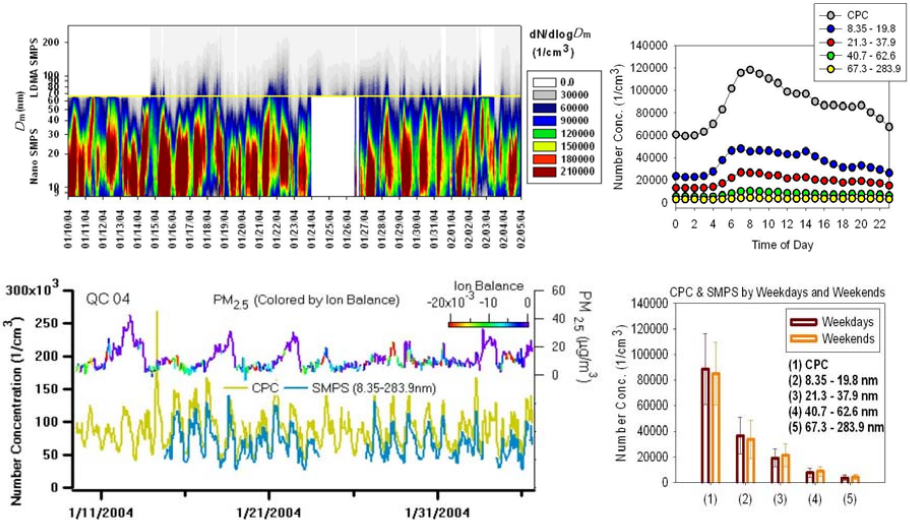


**Fig. 7.** Evolution of particle size distributions and particle concentrations ($dN/d\log D_m$) ($1/cm^3$), time series traces for the hourly number concentration ($1/cm^3$) measured by the CPC (dark yellow line) and SMPS (8.35–283.9 nm) (dark blue line), as well as $PM_{2.5}$ mass concentrations (colored by the ion charge balance), hour-of-day series by CPC (gray) and SMPS (8.35–19.8 nm: blue, 21.3–37.9: red, 40.7–62.6: green, 67.3–283.9: yellow) and weekdays (brown) and weekends (orange) in number concentrations for the QC04.

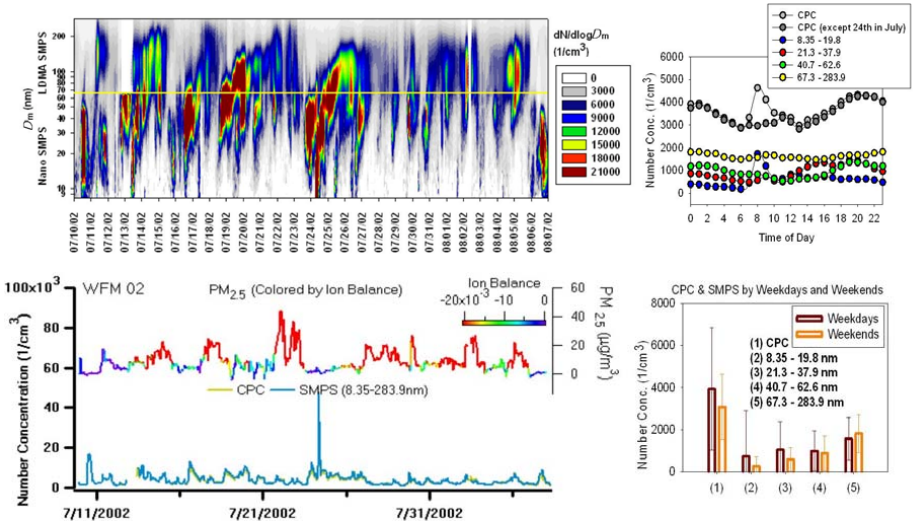


**Fig. 8.** Evolution of particle size distributions and particle concentrations (dN/dlog$D_m$) (1/cm$^3$) and time series traces for the hourly number concentration (1/cm$^3$) measured by the CPC (dark yellow line) and SMPS (8.35–283.9 nm) (dark blue line), as well as $PM_{2.5}$ mass concentrations (colored by the ion charge balance), hour-of-day series by CPC (gray) and SMPS (8.35–19.8 nm: blue, 21.3–37.9: red, 40.7–62.6: green, 67.3–283.9: yellow) and weekdays (brown) and weekends (orange) in number concentrations for the WFM02.

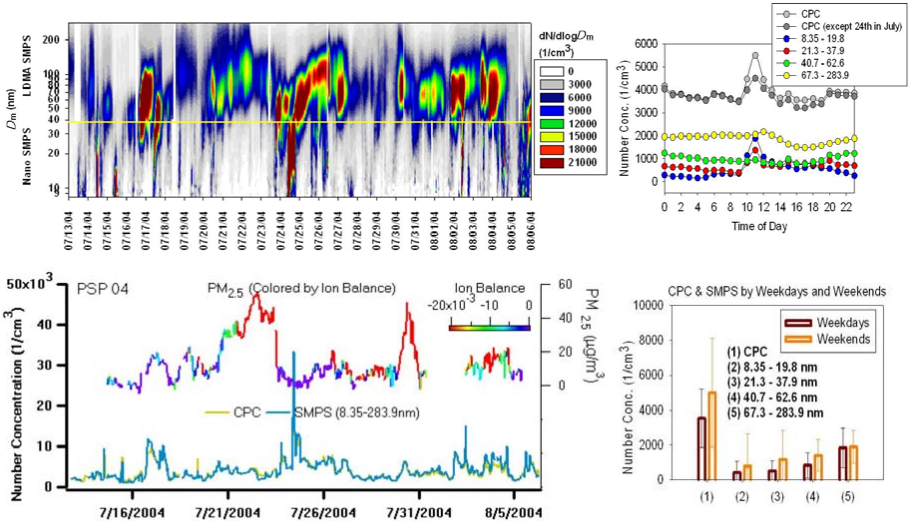


**Fig. 9.** Evolution of particle size distributions and particle concentrations (dN/dlog$D_m$) (1/cm$^3$) and time series traces for the hourly number concentration (1/cm$^3$) measured by the CPC (dark yellow line) and SMPS (8.35–283.9 nm) (dark blue line), as well as $PM_{2.5}$ mass concentrations (colored by the ion charge balance), hour-of-day series by CPC (gray) and SMPS (8.35–19.8 nm: blue, 21.3–37.9: red, 40.7–62.6: green, 67.3–283.9: yellow) and weekdays (brown) and weekends (orange) in number concentrations for the PSP04.

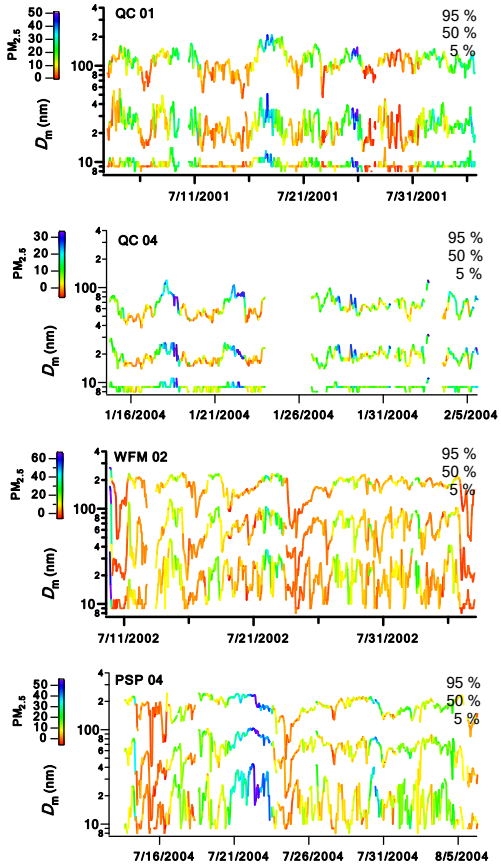


**Fig. 10.** Time series traces for the 95%, 50%, 5% of the particle size diameter (nm) measured by the SMPS [8.35–283.9 nm] colored by $PM_{2.5}$ mass concentrations ($\mu g/m^3$) for the QC01, QC04, WFM02, and PSP04 campaigns.

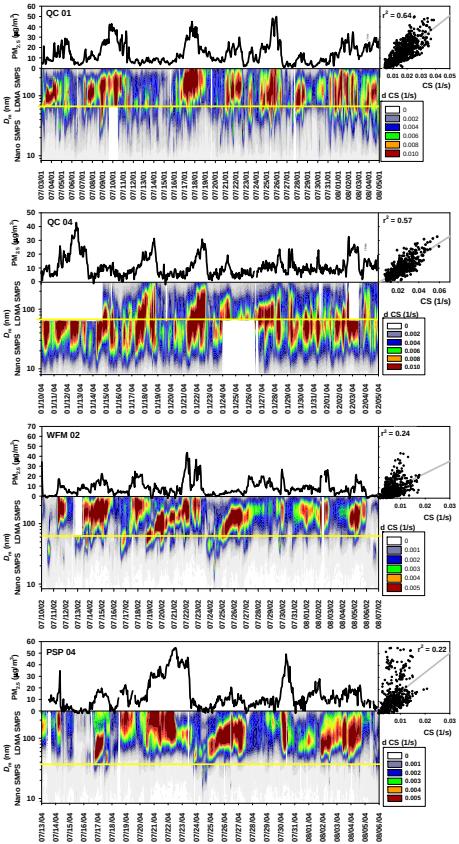


**Fig. 11.** Evolution of particle size distributions and condensation sink (1/s), time series traces for the hourly $PM_{2.5}$ mass concentration ($\mu g/cm^3$), and pairwise correlation scatterplots between $PM_{2.5}$ mass concentration and condensation sink for the QC 01, QC 04, WFM 02 and PSP 04.